



## Influence of carbon support properties in the hydrodeoxygenation of vanillin as lignin model compound

Shahram Alijani<sup>a</sup>, Sofia Capelli<sup>a</sup>, Claudio Evangelisti<sup>b</sup>, Laura Prati<sup>a</sup>, Alberto Villa<sup>a</sup>, Stefano Cattaneo<sup>a,\*</sup>

<sup>a</sup> Università degli Studi di Milano, Dipartimento di Chimica, Via Golgi 19, 20133, Milano, Italy

<sup>b</sup> ISTM-Institute of Molecular Sciences and Technologies, CNR - National Research Council, 20138, Milan, Italy

### ARTICLE INFO

#### Keywords:

Palladium  
Carbon  
Vanillin  
Hydrogenation  
Hydrodeoxygenation

### ABSTRACT

Hydrodeoxygenation of lignin is a fundamental step in biomass valorisation for the reduction of the oxygen content and the synthesis of a wide range of products. Vanillin is a lignin model compound containing an aldehydic group attached to an aromatic ring. Pd nanoparticles are particularly active in the hydrogenation of carbonyl groups and the subsequent hydrogenolysis of the alcoholic bond, especially when the nanoparticles are supported on carbon-based materials. This work aims to study the effect of carbonaceous supports with different chemical-physical properties on both activity and selectivity in the hydrogenation of vanillin to vanillyl alcohol and the subsequent hydrodeoxygenation to creosol. Pd nanoparticles were synthesised by sol immobilisation technique and deposited on four supports (three activated carbons – Norit, KB and G60 – and a carbon nanofiber – HHT) with different graphitisation order and oxygen functionalisation. The catalysts were thoroughly characterised with transmission electron microscopy, X-ray photoelectron spectroscopy and N<sub>2</sub> adsorption. The conversion of vanillin was correlated to the carbon graphitisation order and the concentration of oxygen functionalities of the support, while the production of ether through reaction between vanillyl alcohol and the solvent (isopropanol) was correlated to the presence of carboxylic groups on the support surface. Full conversion to creosol was obtained with all the catalysts in short reaction times (Pd/G60, creosol yield > 99.5 %) and in mild reaction conditions. In addition, the Pd/HHT catalyst showed good stability upon reuse in 5 consecutive reactions.

### 1. Introduction

The world fossil fuel consumption is relentlessly increasing, led by the continuous growth in population and the energy demand of emerging large economies [1,2]. In the last 25 years, the oil consumption increased from less than 70 million barrels of oil per day to around 100 million barrels [2]. The resources, however, are not infinite and sooner rather than later we are going to need an alternative for the production of both chemicals and fuels. In this context, biomass-based materials are receiving growing attention from both an academic and industrial point of view, since they represent the most promising green and sustainable alternative to the conventional feedstock [3–5]. Lignin, in particular, is a natural cross-linked phenolic polymer that constitutes around 30 % of lignocellulosic biomass and it represents the second most abundant renewable carbon source on earth after cellulose [6,7]. The structure of lignin is composed of highly functionalised aromatic rings bound together by a combination of C-O and C-C inter-unit linkages [1]. For this

reason, lignin valorisation often pass through a hydrodeoxygenation (HDO) step, where the C-O bonds are broken and the oxygen content of the final product is consequently reduced [8].

HDO of lignin model molecules, such as guaiacol, anisole, phenol and vanillin, has been intensively studied in the past 2 decades [9–18]. Vanillin, in particular, is a phenolic aldehyde containing both a hydroxyl and methoxy group (in position *para* and *meta*, respectively), and it is an important constituent of bio-oil [19]; for these reasons, it represents a good lignin model substrate for HDO reactions. Typically, vanillin HDO pass through a first hydrogenation step of the aldehydic group to form vanillyl alcohol, which is subsequently hydrodeoxygenated to creosol (Fig. 1). The formation of guaiacol and hydrocarbons is also sometimes reported, even though typically under harsh reaction conditions (i.e. 300 °C and 50 bar of H<sub>2</sub>) [20,21]. Homogeneous catalysts can effectively convert vanillin to the desired product [22–24], although heterogeneous catalysts are usually the preferred choice due to their added stability and recyclability.

\* Corresponding author.

E-mail address: [stefano.cattaneo2@unimi.it](mailto:stefano.cattaneo2@unimi.it) (S. Cattaneo).

<https://doi.org/10.1016/j.cattod.2020.04.026>

Received 15 January 2020; Received in revised form 19 March 2020; Accepted 6 April 2020

0920-5861/ © 2020 Elsevier B.V. All rights reserved.

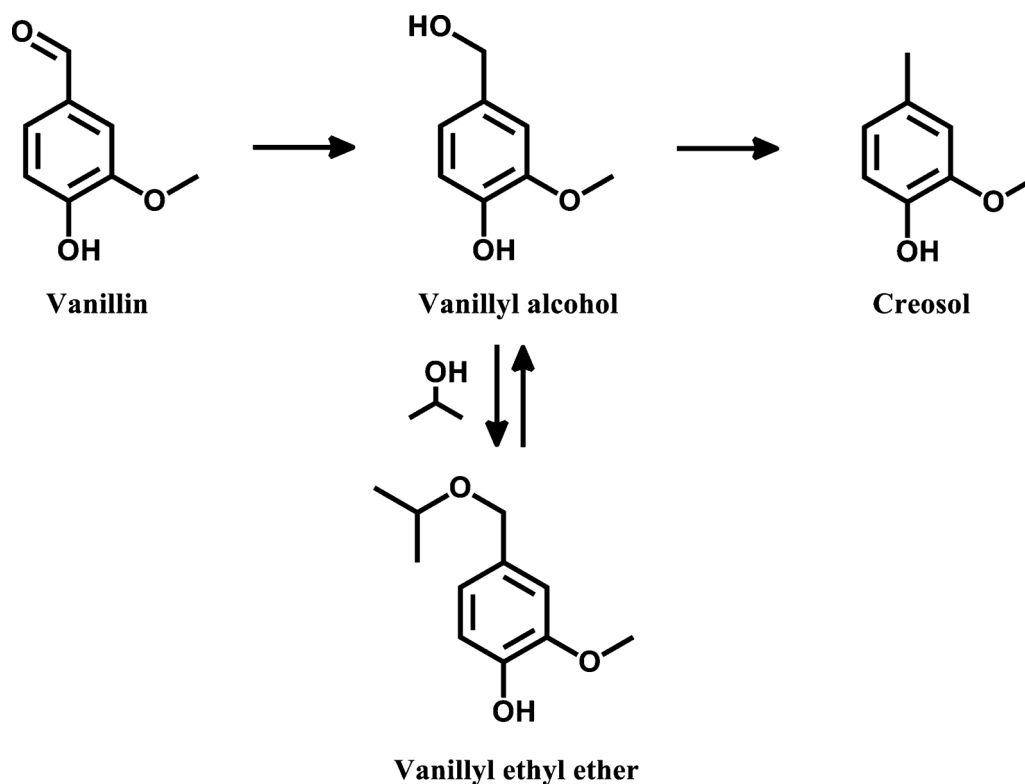


Fig. 1. Vanillin hydrogenation/hydrodeoxygenation pathway.

Supported noble metal nanoparticles, such as Pd [25], Ru [19], Au [26] and Pt [27], showed in recent studies high activity and selectivity to creosol. 96 % of yield was for example achieved by Yang and co-workers using Ru nanoparticles supported on carbon nanotubes [28], while 98 % of selectivity was reached at 99 % vanillin conversion by Jang et al. using Pd nanoparticles on a carbon nitride support in mild reaction conditions (70 °C and 10 bar of H<sub>2</sub>) [29]. A common trait can be identified from the several studies reported in literature on vanillin HDO: the preferred supports for metal nanoparticles are carbonaceous materials, due to their high activity and selectivity displayed [15–18,26–30].

Carbon-based materials such as activated carbons, carbon blacks, graphite, nanotubes and nanofibers have been used for decades in heterogeneous catalysis as support for metal nanoparticles due to their high surface area, high thermal stability in reducing atmosphere and their ability to facilitate the deposition of nanoparticles on surfaces that do not exhibit acid-base properties [31]. In addition, the recovery and recycling of the deposited metal is much easier compared to metal oxides based supports, as carbon materials can be burned off simply by heat treatment in oxidative atmosphere. However, compared to the predominant applications of carbonaceous materials (i.e. adsorbents for gas and water purification), their use in catalysis represents only a moderate share [31]. Carbonaceous-based materials have been successfully employed in the vanillin HDO. Bindwal and co-workers, for example, reported the production of vanillyl alcohol with a selectivity up to 91 % at 95 % of conversion using a commercial 5 wt% Ru/C catalyst in a slurry reactor [19]. Almost full conversion of vanillin into the desired product (creosol) was reached by Yang and colleagues using either Ru nanoparticles or Au nanoparticles supported on carbon nanotubes (CNT) [26,28]. Both metals, however, required high reaction temperature (150 °C) and the use of a toxic and hazardous solvent (decalin). Milder reaction conditions can be achieved employing Pd as active metal. An almost quantitative conversion of vanillin to creosol (98 % yield), for example, was achieved by Jiang and co-workers using Pd nanoparticles supported on mesoporous carbon nitride at 70 °C and

10 bar of H<sub>2</sub> [29]. Most recently, Santos and colleagues obtained 95 % of selectivity to creosol using a Pd/C catalyst in water (100 °C and 30 bar H<sub>2</sub>), although the authors reported a 30 % mass loss due to the formation of oligomers, probably due to the high pressure involved [27,32].

The choice of the appropriate carbonaceous support is extremely important, as already highlighted for several reactions of industrial and academic relevance, such as hydrogenation and oxidation of biomass-derived substrates [33–35], dehydrogenation of cinnamaldehyde [36], and many other reactions [37–40]. In this study, four types of carbonaceous materials with different chemical-physical properties have been employed as support for Pd nanoparticles and tested in the reaction of HDO of vanillin in mild reaction conditions (50 °C, 5 bar of H<sub>2</sub> and isopropanol as a solvent). The catalysts were thoroughly characterised with transmission electron microscopy (TEM), X-ray photoelectron spectroscopy (XPS) and N<sub>2</sub> adsorption (BET) in order to correlate the catalyst surface properties with the catalytic activity and selectivity towards the desired products. Finally, recycle tests were performed on the most active catalyst in order to assess the reusability of the used material.

## 2. Experimental

### 2.1. Materials

Sodium tetrachloropalladate (II) (99.99 %), polyvinyl alcohol (87–89 % hydrolysed) and sodium borohydride (99.99 %) were purchased from Merck. The four different carbonaceous supports were: Cabot Norit (Norit), Darco KB (KB), Darco G60 (G60), and Pyrograf-III carbon nanofiber PR-24 (HHT). For the catalytic reactions, vanillin (99 %, Merck) and isopropanol (99.8 %, Merck) were used.

### 2.2. Catalyst synthesis

Pd nanoparticles were synthesised and supported on four different

carbonaceous materials (namely Norit, KB, G60 and HHT) by sol immobilization method (metal loading of 1 wt%)[41]. The supports have different physical-chemical properties such as surface area, pore size and type of surface functionalities. Pd colloids were prepared adding solution of the metal precursor ( $\text{Na}_2\text{PdCl}_4$ , 1 mL of a  $1.26 \times 10^{-4}$  mol  $\text{L}^{-1}$  solution) to the solution containing polyvinyl alcohol (PVA) as the capping agent (1 wt. % solution, PVA/Pd (wt/wt) = 0.5) to 400 mL of milliQ water.  $\text{NaBH}_4$  (3.7 mL of a 0.1 mol  $\text{L}^{-1}$  solution;  $\text{NaBH}_4/\text{Pd}$  (mol/mol) = 8) was then added to the yellow-brown solution under stirring and left for 30 minutes to accomplish full reduction of the Pd species. Then, the support was added to the colloidal solution under vigorous stirring. The catalyst slurry was acidified to pH 2 adding sulphuric acid before being stirred for 60 min to attain full immobilisation of the metal nanoparticles onto the carbon supports [42]. The catalyst slurries were finally filtered, washed thoroughly with 1 L of distilled water, and dried at 80 °C for 2 h in oven.

### 2.3. Catalyst characterisation

Quantachrome Autosorb was used to measure surface area and pore size. The samples were degassed at 120 °C for 3 h before starting the measurements. All the surface areas were evaluated using Brunauer-Emmett-Teller (BET) method in the partial pressure range  $p/p^\circ$  of 0.05–0.35. The pores volume was calculated using single point method at  $p/p^\circ$  of 0.99.

ZEISS LIBRA200FE microscope operating at 200 kV was used to perform transmission electron microscopy (TEM) analyses. The samples were prepared by sonicating the catalysts in isopropanol and their further deposition on 300 mesh copper grids coated with carbon film. Particle size distributions (PSD) was obtained counting at least 200 particles. The mean particle diameters ( $d_m$ ) were calculated using the formula  $d_m = \sum d_i n_i / \sum n_i$ , where  $n_i$  is the number of particles of diameter  $d_i$ .

Thermo Scientific K-alpha + spectrometer was used for X-ray photoelectron spectroscopy (XPS) measurements. The samples were analysed using a monochromatic Al x-ray source operating at 72 W, with the signal averaged over an oval-shape area of  $600 \times 400 \mu$ . Data were recorded at 150 eV for survey scans and 40 eV for high resolution (HR) scans with a 1 eV and 0.1 eV step size, respectively. CASAXPS (v2.3.17 PR1.1) was used for the analysis of the data, using Scofield sensitivity factors and energy exponent of -0.6.

### 2.4. Catalytic tests

Stainless-steel autoclave equipped with a heater and a magnetic stirrer was utilised to perform hydrogenation reactions at 5 bar and 50 °C. For each experiment, the desired amount of catalyst (31.5 mg, metal/vanillin = 1/1000 mol/mol) along with a solution of vanillin (10 mL, 0.3 M in isopropanol) were loaded in the reactor. The autoclave was then purged with  $\text{N}_2$  3 times and charged with 5 bar  $\text{H}_2$ . The mixture was heated to 50 °C and the reaction started as soon as the stirring speed was set up to 1200 rpm. During the reaction, the samples were taken at regular intervals from the reactor for gas chromatography analysis (Agilent 6890, equipped with a Zebtron ZB5 60 m x0.32 mm x1  $\mu\text{m}$  column and a FID detector. Temperature programme: 2 min at 100 °C, 15 °C  $\text{min}^{-1}$  up to 170 °C with a hold time of 2 min at 170 °C, 20 °C  $\text{min}^{-1}$  up to 300 °C with a final hold time of 3 min). In particular, the stirring was stopped and the reaction quenched putting the autoclave in an ice bath for a couple of minutes. 500  $\mu\text{L}$  of reaction mixture were withdrawn and centrifuged in order to separate the catalyst. 200  $\mu\text{L}$  of the supernatant were then mixed in a GC vial with 800  $\mu\text{L}$  of a solution of dodecanol (external standard). Response factors of the substrate and products were calculated using a known concentration of standard solutions of the pure compounds, using octanal as external standard.

The conversion was calculated using the following equation

(Equation 1):

$$\text{Conversion (\%)} = \frac{\text{mol}_i - \text{mol}_t}{\text{mol}_i} \cdot 100 \quad (1)$$

Where  $\text{mol}_i$  are the initial moles of vanillin and  $\text{mol}_t$  are the moles after a reaction time “t”. The selectivity was calculated according to Equation 2:

$$\text{Selectivity}_a (\%) = \frac{\text{mol}_a}{\sum \text{mol}_n} \cdot 100 \quad (2)$$

Where  $\text{mol}_a$  are the moles of product “a” and  $\sum \text{mol}_n$  is the sum of the moles of all the other reaction products. The initial catalytic activity normalised on the total amount of active metal was calculated using Equation 3:

$$\text{Activity (h}^{-1}\text{)} = \frac{\text{mol}_i - \text{mol}_5}{\text{mol}_{\text{Pd}}} \cdot \frac{60}{t} \quad (3)$$

Where  $\text{mol}_5$  are the moles after 5 minutes of reaction,  $\text{mol}_{\text{Pd}}$  are the moles of Pd introduced in the reactor and t is the reaction time (5 minutes). The catalytic results were also expressed in term of activity normalised on the number of exposed metal surface atoms (Activity<sub>NS</sub>). The evaluation of the number of exposed Pd atoms was performed assuming that all the nanoparticles have cuboctahedral morphology with cubic close-packed structure. A full-shell nanoparticles model applied in previous studies was then adopted [43,44]. The total number of Pd atoms in the cluster ( $N_T$ ) for a given cluster size can be calculated using Equation 4:

$$d_{\text{sph}} = 1.105 \cdot d_{\text{at}} \cdot N_T^{\frac{1}{3}} \quad (4)$$

Where  $d_{\text{sph}}$  is the mean diameter of Pd nanoparticles obtained from TEM analyses and  $d_{\text{at}}$  is the atom diameter of Pd (0.274 nm). The number of surface atoms ( $N_S$ ) and n can be calculated from Equations 5 and 6, based on the values of  $N_T$ :

$$N_T = \frac{10n^3 - 15n^2 + 11n - 3}{3} \quad (5)$$

$$N_S = 10n^2 - 20n + 12 \quad (6)$$

Therefore, the Activity<sub>NS</sub> based on the surface atoms can be calculated using Equation 7:

$$\text{Activity}_{\text{NS}} (\text{s}^{-1}) = \frac{\text{Activity}}{A} \quad (7)$$

Where A is the fraction of atoms lying at the surface calculated dividing  $N_S$  by  $N_T$ .

The most active catalyst was then chosen for stability test, and the liquid-phase vanillin HDO was carried out for five consecutive cycles at 50 °C in 5 bar of  $\text{H}_2$  for 10 minutes (ca. 85 % conversion). After each reaction, all the catalyst was recovered simply by filtration and it was reused after drying in an oven at 50 °C for 20 minutes.

## 3. Results and discussion

### 3.1. Catalyst characterisation

Pd nanoparticles were synthesised by sol-immobilisation technique and deposited on four carbonaceous materials with different physical-chemical properties. Norit, KB and G60 are commercial activated carbon powder, while HHT are commercial hollow fishbone pyrolytically stripped carbon nanofibers treated at high temperature in order to increase the graphitisation degree. The final metal loading was assessed with Inductively Coupled Plasma analysis (ICP), and for all the catalysts it was found a value of 1 wt%.

BET analysis was performed on the Pd supported catalysts (Table 1). Pd/Norit catalyst showed the highest surface area (2000  $\text{m}^2/\text{g}$ ) while Pd/HHT the lowest one (40  $\text{m}^2/\text{g}$ ). The average pore radius among all

**Table 1**  
Surface area, total pore volume and average pore radius of the four catalysts.

Sample	Surface area (m <sup>2</sup> /g)	Total pore volume (cm <sup>3</sup> /g)	Average pore diameter (nm)
Pd/Norit	1995	0.80	5.5
Pd/KB	1604	1.59	2.0
Pd/G60	802	0.75	18.7
Pd/HHT	40	1.50	25.4

**Table 2**  
C, Pd and O amount from XPS survey analysis.

Sample		C 1s	Pd 3d	O 1s	Pd/C	O/C
Pd/Norit	B.E. (eV)	284.07	335.08	532.07	0.015	0.169
	Atomic (%)	84.4	1.3	14.3		
Pd/KB	B.E. (eV)	285.08	336.08	533.08	0.017	0.128
	Atomic (%)	87.3	1.4	11.3		
Pd/G60	B.E. (eV)	284.07	335.08	532.07	0.013	0.085
	Atomic (%)	91.1	1.3	7.6		
Pd/HHT	B.E. (eV)	284.19	337.19	532.19	0.002	0.009
	Atomic (%)	98.8	0.3	0.9		

the samples was wide: from 2 nm of Pd/KB to 25.4 nm of Pd/HHT.

XPS analyses were performed on the synthesised catalysts in order to evaluate Pd oxidation state, graphitisation order and the presence and abundance of oxygen functionalities. Survey spectra were recorded and analysed to evaluate the atomic % of the different elements on the catalyst surface (Figure S1). C 1s, Pd 3d and O 1s were considered for the calculation of Pd/C and O/C atomic ratios (Table 2). Pd/Norit, Pd/KB and Pd/G60 showed similar amount of C 1s species (84.4 %, 87.3 %, and 91.1 %, respectively), while Pd/HHT displayed the highest C 1s amount (98.8 %). Pd/Norit, Pd/KB and Pd/G60 presented the same amount of superficial Pd (ca. 1.3 %), while Pd/HHT sample had the lowest exposed Pd amount (0.3 %). The low Pd exposure can be explained considering that the Pd nanoparticles might be distributed prevalently in the inner walls of the carbon nanofibers. Finally, O 1s species were evaluated and, as expected, the Pd/HHT catalyst showed the lowest amount of functionalisation (0.9 %), while Pd/Norit the highest one (14.3 %). The Pd/C ratio was calculated as well, and Pd/KB showed the highest value (0.017), followed by Pd/Norit and Pd/G60 (0.015 and 0.013, respectively). Pd/HHT had the lowest Pd/C ratio (0.002) due to the low amount of particle present on the external catalyst surface. Finally, O/C ratio was evaluated and Pd/HHT exhibited the lowest value (0.009) while Pd/Norit the highest one (0.169).

C 1s high resolution spectra was deconvoluted (Table 3 and Figure S2) and 4 main carbon groups were found: C = C double bond (284.20-204.70 eV), C-C single bond (284.98-285.23 eV), carbonylic groups C = O (286.57-286.97 eV), and C-O ether-like group (288.99-291.76 eV). Pd/Norit catalysts is mainly composed of C-C sp<sup>3</sup> carbon (42.9 %), while regarding oxygen moieties C = O is the highest (19.2 %). Pd/KB has 63.3 % of C = C and 22.9 % of C-C, while carbonyl/

**Table 3**  
C 1s, O 1s and Pd 3d XPS analysis of the four catalysts.

Sample		C 1s				O 1s			Pd 3d			
		C = C (sp <sup>2</sup> )	C-C (sp <sup>3</sup> )	C = O	C-O	C π-π*	C = O	C-OH/C-O-C	COOH	Pd(0)	Pd(II)	Pd(0)/Pd(II)
Pd/Norit	B.E. (eV)	284.20	285.10	286.98	288.9	-	532.00	533.01	535.47	335.45	337.01	1.41
	Atomic (%)	28.0	42.9	19.2	9.9	-	32.2	62.7	5.1	58.5	41.5	
Pd/KB	B.E. (eV)	284.29	284.98	287.19	288.99	290.78	530.98	532.65	535.87	335.23	336.89	0.30
	Atomic (%)	63.6	22.9	5.9	4.9	2.7	19.6	64.2	16.2	75.2	23.8	
Pd/G60	B.E. (eV)	284.30	285.21	286.57	289.10	-	531.89	533.34	535.58	335.50	337.41	1.11
	Atomic (%)	55.5	24.3	14.8	5.4	-	20.5	58.4	21.1	52.7	47.3	
Pd/HHT	B.E. (eV)	284.70	285.23	286.97	291.76	291.19	531.78	533.36	535.53	335.20	336.84	1.17
	Atomic (%)	82.1	7.5	2.1	0.43	7.9	53.3	28.52	18.2	54	46	

carboxylic groups and ether/hydroxyl-like group were 5.9 % and 4.9 %, respectively. Pd/G60 showed similar results, although the C = O contribution increased to 14.8 %. Pd/HHT catalyst showed the highest amount of C = C (82.1 %), therefore the support can be considered highly graphitised. Graphitisation is also confirmed by the presence of high percentage of π-π\* group (7.9 %), which is typical of large conjugated systems.

The deconvolution of high-resolution spectra of O 1s (Table 3 and Figure S3) showed the presence of 3 different groups: carbonylic groups C = O (530.98 -532.00 eV), C-OH/C-O-C (532.65-533.36 eV), and carbonylic group COOH (535.47-535.87 eV). The main group was C-OH/C-O-C (58.4-64.2 %) except for Pd/HHT sample (28.52 %), where the most important moiety was C = O (53.3 %).

Regarding Pd 3d high-resolution spectra, two oxidation states of Pd were found (Table 3 and Figure S4). The peak at 335.20-335.50 eV was assigned to Pd(0), while the one at 336.84-337.41 eV was ascribed to Pd(II). Pd(0)/Pd(II) ratio was calculated and Pd/G60 and Pd/HHT samples showed similar value (1.11 and 1.17, respectively). Pd/KB exhibited the lowest ratio (0.30), while Pd/Norit the highest one (1.41).

TEM analyses were performed to evaluate the mean particle size diameter and size distribution (Fig. 2). In all the samples, the nanoparticles are homogeneously dispersed on the supports. Pd/Norit and Pd/KB presented similar mean Pd particle size (2.5 and 2.7 nm, respectively). Pd/G60 and Pd/HHT, on the other hand, showed higher Pd nanoparticle mean diameters (3.5 and 3.9 nm, respectively). The particle size distribution is similar for the Pd/Norit, Pd/KB and Pd/G60 catalysts (in a 0.6 – 0.8 nm range), while slightly larger for the Pd/HHT (± 1.2 nm). These differences in particle size cannot be attributed to the synthetic procedure, since the metal nanoparticles were synthesised with the same procedure. Weak interaction between the metal colloid and the support leads to particle agglomeration and coalescence. On the carbon surface, metal nanoparticles are anchored either on structural defects (such as edges and kinks in the graphitic planes or in the amorphous C sp<sup>3</sup> structure) or on heteroatomic functional groups (such as oxygen functionalities). Although the quantification of structural defects is not trivial, an indication of the metal-support strength can be inferred by the amount of oxygen species from XPS analysis. As expected, larger nanoparticles were obtained with low functionalised carbons (HHT and G60), while smaller nanoparticles were obtained with the highly functionalised supports (Norit and KB).

### 3.2. Vanillin hydrodeoxygenation

The as characterised catalysts were tested and compared in the vanillin hydrodeoxygenation reaction (HDO). The reaction conditions chosen were 50 °C and 5 bar of H<sub>2</sub>, using isopropanol as a solvent (vanillin concentration of 0.3 mol L<sup>-1</sup>; Pd/vanillin molar ratio of 1/1000). In these reaction conditions, using a Pd-based catalyst, vanillin typically undergoes a first hydrogenation step, yielding vanillyl alcohol (Fig. 1). Vanillyl alcohol is then further converted to creosol through a hydrogenolysis step. Despite the use of a secondary alcohol as solvent, hydrogen transfer mechanism was avoided due to the low temperature

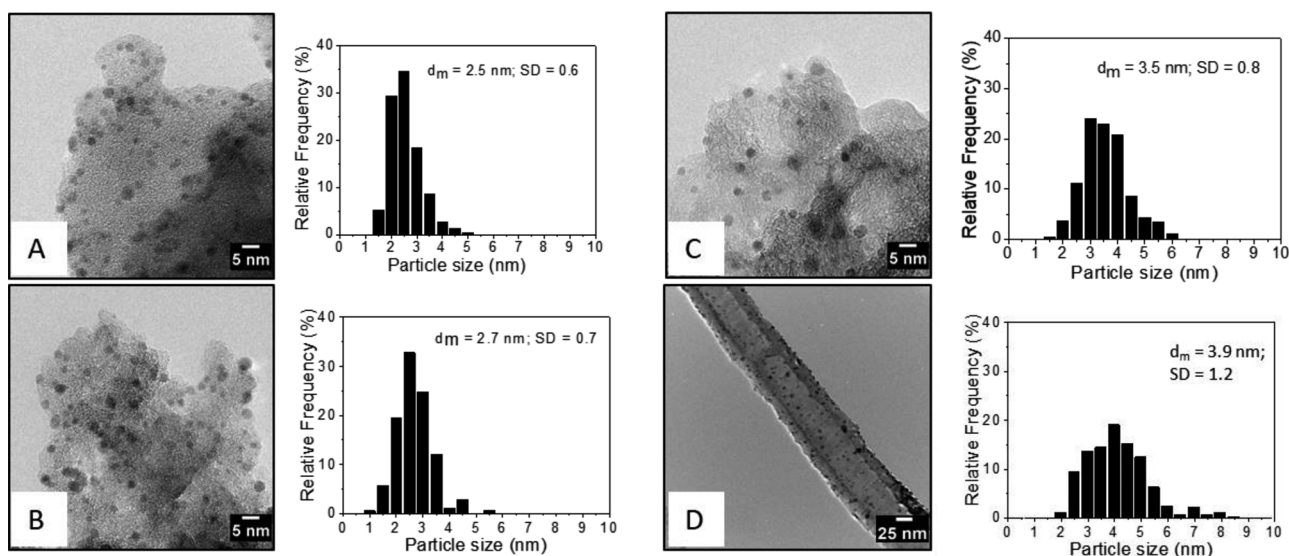


Fig. 2. Representative TEM micrographs with relative particle size distribution of the four catalysts: A) Pd/Norit, B) Pd/KB, C) Pd/G60, and D) Pd/HHT.

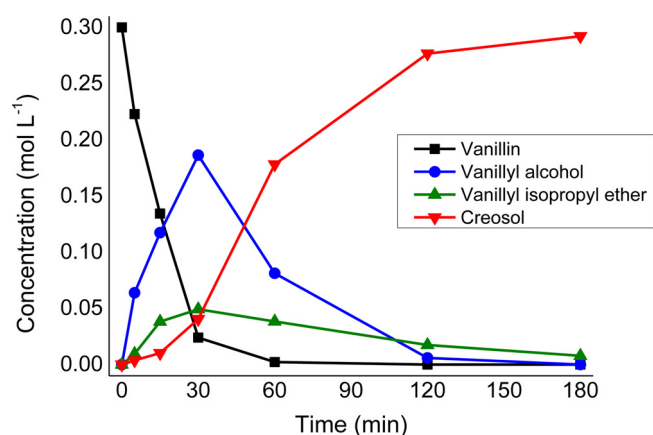


Fig. 3. Vanillin hydrodeoxygenation reaction profile with the Pd/KB catalyst. Reaction conditions: 50 °C, 5 bar of H<sub>2</sub>, vanillin concentration 0.3 mol L<sup>-1</sup> in isopropanol, Pd/vanillin molar ratio 1/1000.

at which the reactions were carried out. In order to confirm this, a reaction was carried out in absence of H<sub>2</sub> (5 bar of N<sub>2</sub>) and no product formation was observed. Fig. 3 shows the reaction profile of vanillin HDO carried out using Pd/KB as a catalyst. Full conversion was achieved in less than 1 h. The reaction profile shows the features of a typical consecutive reaction, with vanillyl alcohol as the intermediate product. Interesting, an additional product was detected in the reaction mixture, namely vanillyl isopropyl ether. The ether is produced by reaction of vanillyl alcohol with a molecule of solvent (isopropanol) and it is consumed with time since it is in equilibrium with the alcohol (Fig. 1).

The four synthesised catalysts showed different initial activity (calculated after 5 minutes of reaction) as shown in Table 4 (full reaction profiles in the Supporting Information). The activity of the Pd/KB and Pd/G60 were very similar (2816 h<sup>-1</sup> and 2804 h<sup>-1</sup>, respectively) and almost three times as high compared to the Pd/Norit catalyst (initial activity of 971 h<sup>-1</sup>). Pd/HHT, on the other hand, showed the highest activity among the catalysts tested (3196 h<sup>-1</sup>). These activity values, however, are calculated considering the whole amount of Pd present in the reaction mixture (see Experimental section). Nevertheless, only the exposed Pd atoms actively take part in the catalysis. For this reason, the catalytic activity was compared using the normalised initial activity (Activity<sub>NS</sub>), which is the catalytic activity normalised by the number of

Table 4

Activity and selectivity of the four catalysts. Reaction conditions: 50 °C, 5 bar of H<sub>2</sub>, vanillin concentration 0.3 mol L<sup>-1</sup> in isopropanol, Pd/vanillin molar ratio 1/1000. Selectivity calculated at 50 % conversion.

Sample	Activity (s <sup>-1</sup> )	Activity <sub>NS</sub> (s <sup>-1</sup> )	Selectivity (%)		
			Vanillyl alcohol	Ether	Creosol
Pd/Norit	971	2163	80	9	11
Pd/KB	2816	6677	73	21	6
Pd/G60	2804	8269	56	23	21
Pd/HHT	3196	10355	82	5	13

exposed Pd atoms (see Experimental section). This parameter thus allows the comparison of catalysts having different mean particle size. The newly calculated Activity<sub>NS</sub> values showed a similar trend, with Pd/Norit and Pd/HHT being the least and the most active catalysts (2163 h<sup>-1</sup> and 10355 h<sup>-1</sup>, respectively). On the other hand, a clear distinction between the Pd/KB and Pd/G60 catalysts in terms of activity is now visible (6677 h<sup>-1</sup> and 8269 h<sup>-1</sup>, respectively). The rate of conversion of vanillin is therefore dependent not only on the particle size, but also on other features of the catalysts.

The Activity<sub>NS</sub> values obtained could not be correlated with the Pd exposure calculated by XPS. Despite being the catalyst with lower Pd exposure, in fact, the Pd/HHT catalyst showed the highest activity. This indicates that most of the nanoparticles are easily accessible to the substrate in the reaction conditions studied. Also the Pd oxidation state does not seem to be correlated to the overall catalytic activity. This, however, is not unexpected, since it is known that Pd oxidation state can change *in-situ* in the reaction conditions used [45].

Plotting the Activity<sub>NS</sub> values versus the degree of graphitisation of the support (expressed by the amount of C-C sp<sup>2</sup>-hybridised carbon obtained by XPS analysis, more information in the Supporting Information), for example, a linear correlation can be noticed (Fig. 4). In particular, the rate of conversion of vanillin increases with increasing degree of graphitisation. These results can be explained by the strong interaction between the graphitic plane of the support and the aromatic ring of the substrate that allows a better interaction with the active metal nanoparticles. It has been in fact previously reported that the substrate is weakly adsorbed on the catalyst sites for a similar vanillin-Ru/C system [19]. At the same time, a linear correlation can be found also plotting the Activity<sub>NS</sub> versus the concentration of oxygen functionalities of the support (expressed by the O/C molar ratio obtained by

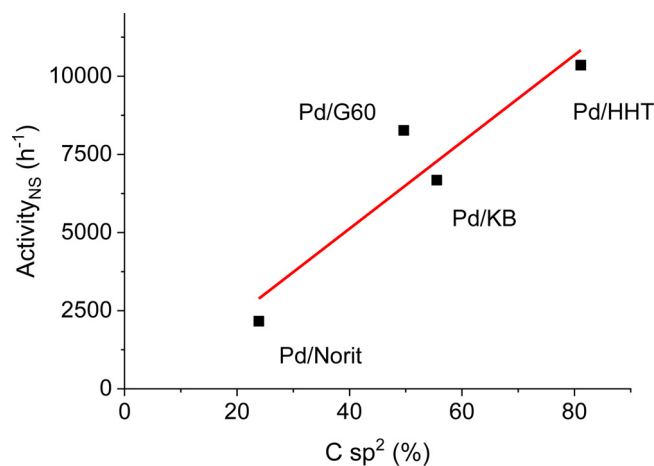


Fig. 4. Correlation between activity<sub>NS</sub> and the graphitisation order (C sp<sup>2</sup>).

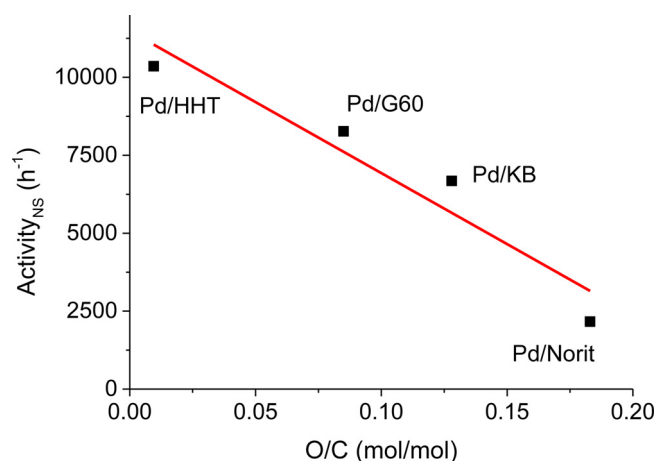


Fig. 5. Correlation between activity<sub>NS</sub> and the amount of oxygen species on the catalysts surface.

XPS analysis, Fig. 5). Also in this case, the responsible for the change in activity is the support-substrate interaction; an increase of the oxygen functionalities, in fact, disrupts the graphitic plane structure of the support. The activity in the vanillin hydrogenation reaction therefore decreases with an increase in oxygen content at the carbon surface. Similar results were recently obtained in the hydrogenation of cinnamaldehyde [36,46].

The selectivity is affected by the type of carbonaceous material used as well (Table 4 and Figure S5-7). Despite a previous report showing mass loss up to 30 % with a similar Pd/C catalyst [27], the sum of reactant and products masses from GC analysis was always close to 100 %; therefore no mass loss was observed across the range of conversion studied. Comparing the selectivity at 50 % conversion, high amount of vanillyl alcohol was produced with Pd/Norit (80 % of selectivity), despite this catalyst being the least active of the series. High selectivity towards the alcohol was reached also by the Pd/HHT and Pd/KB catalysts (82 % and 73 %, respectively), while only 56 % of vanillin was converted into vanillyl alcohol by the Pd/G60. The latter catalyst was the only one producing significant amount of vanillyl isopropyl ether (23 %). Although a comprehensive correlation between the selectivity towards the various products with the support's features is not clear from the gathered data, the ether formation can be associated with the amount of carboxylic functionalities on the support (COOH groups, see Supporting Information for the calculation). As expected, in fact, decreasing the acidic functionality of the support, the alcohol-ether equilibrium shifts towards vanillyl alcohol (Fig. 6).

Once the reaction reaches completion, the only product detected

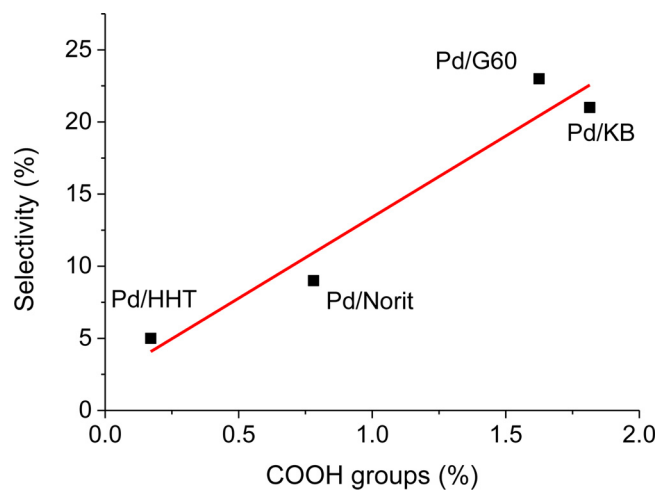


Fig. 6. Correlation between selectivity towards vanillyl isopropyl ether and the concentration of carboxylic functionalities on the catalysts surface.

was in all the cases creosol (Fig. 3 and S8-10, selectivity > 99.5 %). This result puts these materials among the most active and selective catalysts reported in literature (Table 5), especially considering the mild reaction conditions at which the reactions were conducted (50 °C, 5 bar H<sub>2</sub> and metal/substrate of 1/1000 mol/mol).

Recycling tests were performed on the most active catalyst: Pd/HHT (Fig. 7). As described in the Experimental Section, after every reaction the reaction mixture was filtrated and the catalyst reused as is without any washing step. After 5 consecutive reactions, the conversion did not decrease significantly, confirming the high stability of the catalyst. Similarly, the selectivity to vanillyl alcohol remained nearly constant, varying in a 73 - 76 % range.

#### 4. Conclusion

Four different carbonaceous materials (three activated carbons – Norit, KB and G60 – and a carbon nanofiber – HHT) were effectively used as support for Pd nanoparticles and employed in the hydrodeoxygenation of vanillin. The activity was correlated to the graphitisation order and the concentration of oxygen functionalities of the support. In particular, increasing the graphitisation order the activity increased due to a strong interaction between the graphitic plane of the support and the aromatic ring of the substrate, that allows a better interaction with the active metal nanoparticles. Similarly, the presence of oxygen functionalities on the support surface disrupts the graphitic plane structure of the support and therefore decreases the reaction rate.

Full conversion to creosol was obtained with all the catalysts in short reaction times (Pd/G60, creosol yield > 99.5 %) and in mild reaction conditions. The support, however, affected the selectivity at lower conversion. At 50 % of conversion, in fact, vanillyl alcohol was the main product of Pd/Norit, Pd/HHT and Pd/KB (selectivity in the 73 - 82 % range), while Pd/G60 produced high amount of both vanillyl isopropyl ether and creosol (23 and 21 % respectively). The formation of ether was correlated to the amount of carboxylic functionalities on the support (COOH groups), with high quantity of ether produced with supports containing high number of carboxylic groups. Finally, the Pd/HHT catalyst showed good stability upon recycling, maintaining both activity and selectivity for 5 consecutive reactions.

#### Statement

Shahram Alijani synthesised the catalysts, carried out catalytic evaluation and helped in the writing of the manuscript. Sofia Capelli helped in designing the experiments and carried out XPS experiments, helping with the interpretation and the writing of the manuscript.

**Table 5**

Main results from vanillin hydrodeoxygenation over Pd-based catalysts reported in literature and compared to ours.

Sample	Reaction conditions	Conversion (%)	Selectivity <sub>Creosol</sub> (%)	Ref.
Zn/Pd/C	150 °C, 20 bar, methanol	> 99 (8 h)	81	[14]
Pd/C	110 °C, 10 bar, water	> 99.5 (2 h)	79	[25]
Pd/MMF	110 °C, 10 bar, water	> 99.5 (2 h)	71	[25]
Pd/TiO <sub>2</sub>	110 °C, 10 bar, water	> 99.5 (2 h)	17	[25]
Pd/ $\gamma$ -Al <sub>2</sub> O <sub>3</sub>	110 °C, 10 bar, water	> 99.5 (2 h)	67	[25]
Pd/MSMF	110 °C, 10 bar, water	> 99.5 (2 h)	> 99.5	[25]
Pd/C	100 °C, 10 bar, octane-water	> 99 (3 h)	94	[28]
Pd-carbon nitride	70 °C, 10 bar, water	99 (1 h)	99	[29]
Pd/C	100 °C, 30 bar, water	100 (3 h)	95 (30 % mass loss)	[27]
Pd/Norit	50 °C, 5 bar, isopropanol	100 (5 h)	> 99.5	This work
Pd/HHT	50 °C, 5 bar, isopropanol	100 (4 h)	> 99.5	This work
Pd/KB	50 °C, 5 bar, isopropanol	100 (3 h)	> 99.5	This work
Pd/G60	50 °C, 5 bar, isopropanol	100 (1 h)	> 99.5	This work

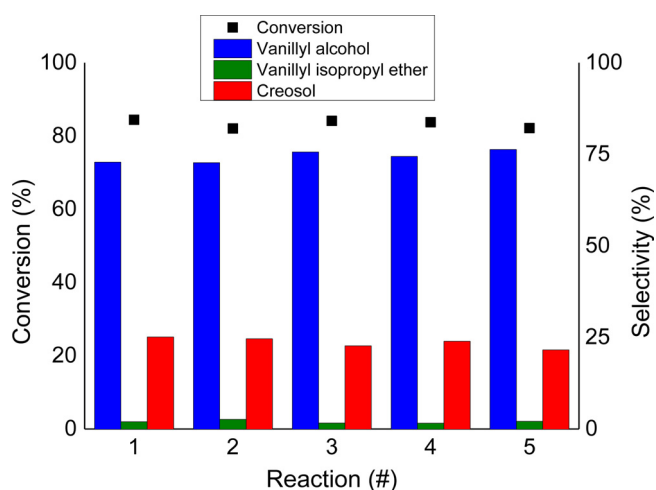


Fig. 7. Stability test of the Pd/HHT catalyst over 5 consecutive reactions. Reaction conditions: 50 °C, 5 bar of H<sub>2</sub>, vanillin concentration 0.3 mol L<sup>-1</sup> in isopropanol, Pd/vanillin molar ratio 1/1000, reaction time 10 minutes.

Claudio Evangelisti carried out TEM analysis and helped with the interpretation. Laura Prati and Alberto Villa were involved in the writing and editing of the manuscript. Stefano Cattaneo designed the experiments, wrote the article and was involved in the editing of the manuscript.

#### Declaration of Competing Interest

The authors declare that they have no known competing financial interests or personal relationships that could have appeared to influence the work reported in this paper.

#### Appendix A. Supplementary data

Supplementary material related to this article can be found, in the online version, at doi:<https://doi.org/10.1016/j.cattod.2020.04.026>.

#### References

- [1] S. Guadix-Montero, M. Sankar, Review on Catalytic Cleavage of C–C Inter-unit Linkages in Lignin Model Compounds: Towards Lignin Depolymerisation, *Top. Catal.* 61 (2018) 183–198.
- [2] BP Statistical Review of World Energy 2018, (2018).
- [3] J.B. Binder, R.T. Raines, Simple Chemical Transformation of Lignocellulosic Biomass into Furans for Fuels and Chemicals, *J. Am. Chem. Soc.* 131 (2009) 1879–1985.
- [4] M.J.C. van der Stelt, H. Gerhauser, J.H.A. Kiel, K.J. Ptasinski, Biomass upgrading by torrefaction for the production of biofuels: A review, *Biomass and Bioenergy.* 35 (2011) 3748–3762.
- [5] A. Demirbas, Biorefinery Technologies for Biomass Upgrading, *Energy Sources, Part*

- [6] A Recover, *Util. Environ. Eff.* 32 (2010) 1547–1558.
- [6] M. Stucchi, S. Cattaneo, A. Cappella, W. Wang, D. Wang, A. Villa, L. Prati, Catalytic Oxidation of Methoxy Substituted Benzyl Alcohols as Model for Lignin Valorisation, *Catal. Today.* (2019) 0–1.
- [7] J.D. Gargulak, S.E. Lebo, T.J. McNally, Lignin, *Kirk-Othmer Encycl. Chem. Technol.* (2015) 1–26.
- [8] P. Mäki-Arvela, D.Y. Murzin, Hydrodeoxygenation of lignin-derived phenols: From fundamental studies towards industrial applications, *Catalysts.* 7 (2017).
- [9] Q. Lu, C.-J. Chen, W. Luc, J.G. Chen, A. Bhan, F. Jiao, Ordered Mesoporous Metal Carbides with Enhanced Anisole Hydrodeoxygenation Selectivity, *ACS Catal.* 6 (2016) 3506–3514.
- [10] M. Lu, J. Zhu, M. Li, Y. Shan, M. He, C. Song, TiO<sub>2</sub>-Modified Pd/SiO<sub>2</sub> for Catalytic Hydrodeoxygenation of Guaiacol, *Energy & Fuels.* 30 (2016) 6671–6676.
- [11] R. Lødeng, C. Ranga, T. Rajkhowa, V.I. Alexiadis, H. Bjorkan, S. Chytil, I.H. Svenum, J. Walmsley, J.W. Thybaut, Hydrodeoxygenation of phenolics in liquid phase over supported MoO<sub>3</sub> and carburized analogues, *Biomass Convers. Biorefinery.* 7 (2017) 343–359.
- [12] F. Jiang, J. Cai, B. Liu, Y. Xu, X. Liu, Particle size effects in the selective hydrogenation of cinnamaldehyde over supported palladium catalysts, *RSC Adv.* 6 (2016) 75541–75551.
- [13] X. Wan, C. Zhou, J. Chen, W. Deng, Q. Zhang, Y. Yang, Y. Wang, Base-free aerobic oxidation of 5-hydroxymethyl-furfural to 2,5-furandicarboxylic acid in water catalyzed by functionalized carbon nanotube-supported au-pd alloy nanoparticles, *ACS Catal.* 4 (2014) 2175–2185.
- [14] T.H. Parsell, B.C. Owen, I. Klein, T.M. Jarrell, C.L. Marcum, L.J. Hauptert, L.M. Amundson, H.I. Kenttämää, F. Ribeiro, J.T. Miller, M.M. Abu-Omar, Cleavage and hydrodeoxygenation (HDO) of C–O bonds relevant to lignin conversion using Pd/Zn synergistic catalysis, *Chem. Sci.* 4 (2013) 806–813.
- [15] Z. Zhu, H. Tan, J. Wang, S. Yu, K. Zhou, Hydrodeoxygenation of vanillin as a bio-oil model over carbonaceous microspheres-supported Pd catalysts in the aqueous phase and Pickering emulsions, *Green Chem.* 16 (2014) 2636–2643.
- [16] L. Jiang, P. Zhou, C. Liao, Z. Zhang, S. Jin, Cobalt Nanoparticles Supported on Nitrogen-Doped Carbon: An Effective Non-Noble Metal Catalyst for the Upgrade of Biofuels, *ChemSusChem.* 11 (2018) 959–964.
- [17] L. He, Y. Qin, H. Lou, P. Chen, Highly dispersed molybdenum carbide nanoparticles supported on activated carbon as an efficient catalyst for the hydrodeoxygenation of vanillin, *RSC Adv.* 5 (2015) 43141–43147.
- [18] H. Yang, R. Nie, W. Xia, X. Yu, D. Jin, X. Lu, D. Zhou, Q. Xia, Co embedded within biomass-derived mesoporous N-doped carbon as an acid-resistant and chemoselective catalyst for transfer hydrodeoxygenation of biomass with formic acid, *Green Chem.* 19 (2017) 5714–5722.
- [19] A.B. Bindwal, P.D. Vaidya, Reaction kinetics of vanillin hydrogenation in aqueous solutions using a Ru/C catalyst, *Energy and Fuels.* 28 (2014) 3357–3362.
- [20] X. Zhang, W. Tang, Q. Zhang, T. Wang, L. Ma, Hydrocarbons Production from Lignin-derived Phenolic Compounds over Ni/SiO<sub>2</sub> Catalyst, *Energy Procedia.* 105 (2017) 518–523.
- [21] A.L. Jongerijs, R. Jastrzebski, P.C.A. Bruijninx, B.M. Weckhuysen, CoMo sulfide-catalyzed hydrodeoxygenation of lignin model compounds: An extended reaction network for the conversion of monomeric and dimeric substrates, *J. Catal.* 285 (2012) 315–323.
- [22] F.H. Mahfud, S. Bussemaker, B.J. Kooi, G.H. Ten Brink, H.J. Heeres, The application of water-soluble ruthenium catalysts for the hydrogenation of the dichloromethane soluble fraction of fast pyrolysis oil and related model compounds in a two phase aqueous–organic system, *J. Mol. Catal. A Chem.* 277 (2007) 127–136.
- [23] F. Huang, W. Li, Q. Lu, X. Zhu, Homogeneous Catalytic Hydrogenation of Bio-Oil and Related Model Aldehydes with RuCl<sub>2</sub>(PPh<sub>3</sub>)<sub>3</sub>, *Chem. Eng. Technol.* 33 (2010) 2082–2088.
- [24] L. Busetto, D. Fabbri, R. Mazzoni, M. Salmi, C. Torri, V. Zanotti, Application of the Shvo catalyst in homogeneous hydrogenation of bio-oil obtained from pyrolysis of white poplar: New mild upgrading conditions, *Fuel.* 90 (2011) 1197–1207.
- [25] Z. Lv, Q. Sun, X. Meng, F.S. Xiao, Superhydrophilic mesoporous sulfonated melamine-formaldehyde resin supported palladium nanoparticles as an efficient catalyst for biofuel upgrade, *J. Mater. Chem. A.* 1 (2013) 8630–8635.
- [26] X. Yang, Y. Liang, X. Zhao, Y. Song, L. Hu, X. Wang, Z. Wang, J. Qiu, Au/CNTs

- catalyst for highly selective hydrodeoxygenation of vanillin at the water/oil interface, *RSC Adv.* 4 (2014) 31932–31936.
- [27] J.L. Santos, M. Alda-Onggar, V. Fedorov, M. Peurla, K. Eränen, P. Mäki-Arvela, M. Centeno, D.Y. Murzin, Hydrodeoxygenation of vanillin over carbon supported metal catalysts, *Appl. Catal. A Gen.* 561 (2018) 137–149.
- [28] X. Yang, Y. Liang, Y. Cheng, W. Song, X. Wang, Z. Wang, J. Qiu, Hydrodeoxygenation of vanillin over carbon nanotube-supported Ru catalysts assembled at the interfaces of emulsion droplets, *Catal. Commun.* 47 (2014) 28–31.
- [29] H. Jiang, X. Yu, X. Peng, H. Zhang, R. Nie, X. Lu, D. Zhou, Q. Xia, Efficient aqueous hydrodeoxygenation of vanillin over a mesoporous carbon nitride-modified Pd nanocatalyst, *RSC Adv.* 6 (2016) 69045–69051.
- [30] R. Nie, H. Yang, H. Zhang, X. Yu, X. Lu, D. Zhou, Q. Xia, Mild-temperature hydrodeoxygenation of vanillin over porous nitrogen-doped carbon black supported nickel nanoparticles, *Green Chem.* 19 (2017) 3126–3134.
- [31] P. Serp, J.L. Figueiredo, Carbon materials for catalysis, (2009).
- [32] J.L. Santos, P. Mäki-Arvela, J. Wärnå, A. Monzón, M.A. Centeno, D.Y. Murzin, Hydrodeoxygenation of vanillin over noble metal catalyst supported on biochars: Part II: Catalytic behaviour, *Appl. Catal. B Environ.* 268 (2020) 118425.
- [33] B. Donoeva, N. Masoud, P.E. de Jongh, Carbon Support Surface Effects in the Gold-Catalyzed Oxidation of 5-Hydroxymethylfurfural, *ACS Catal.* 7 (2017) 4581–4591.
- [34] A. Jouve, S. Cattaneo, S. Capelli, M. Stucchi, C. Evangelisti, A. Villa, L. Prati, CNF-Functionalization as Versatile Tool for Tuning Activity in Cellulose-Derived Product Hydrogenation, *Molecules.* 24 (2019) 316–330.
- [35] S. Cattaneo, H. Nashhajian, F. Somodi, C. Evangelisti, A. Villa, L. Prati, Ruthenium on carbonaceous materials for the selective hydrogenation of HMF, *Molecules.* 23 (2018) 1–13.
- [36] S. Cattaneo, F.J.S. Trujillo, N. Dimitratos, A. Villa, The Effect of Carbon Nanofibers Surface Properties in Hydrogenation and Dehydrogenation Reactions, *Appl. Sci.* 9 (2019) 1–14.
- [37] T. Yoshii, K. Nakatsuka, T. Mizobuchi, Y. Kuwahara, H. Itoi, K. Mori, T. Kyotani, H. Yamashita, Effects of Carbon Support Nanostructures on the Reactivity of a Ru Nanoparticle Catalyst in a Hydrogen Transfer Reaction, *Org. Process Res. Dev.* 22 (2018) 1580–1585.
- [38] X. Tuaeov, S. Rudi, P. Strasser, The impact of the morphology of the carbon support on the activity and stability of nanoparticle fuel cell catalysts, *Catal. Sci. Technol.* 6 (2016) 8276–8288.
- [39] H. Schmies, E. Hornberger, B. Anke, T. Jurzinsky, H.N. Nong, F. Dionigi, S. Kühl, J. Drnc, M. Lerch, C. Cremers, P. Strasser, Impact of Carbon Support Functionalization on the Electrochemical Stability of Pt Fuel Cell Catalysts, *Chem. Mater.* 30 (2018) 7287–7295.
- [40] K.N. Iost, V.A. Borisov, V.L. Temerev, N.S. Smirnova, Y.V. Surovikin, M.V. Trenikhin, A.B. Arbutov, T.I. Gulyaeva, D.A. Shlyapin, P.G. Tsyrunnikov, A.A. Vedyagin, Effect of the carbon support graphitization on the activity and thermal stability of Ru-Ba-Cs/C ammonia decomposition catalysts, *React. Kinet. Mech. Catal.* 127 (2019) 85–102.
- [41] S. Campisi, M. Schiavoni, C.E. Chan-thaw, A. Villa, Untangling the Role of the Capping Agent in Nanocatalysis: Recent Advances and Perspectives, *Catalysts.* 6 (2016) 1–21.
- [42] A. Villa, D. Wang, N. Dimitratos, D. Su, V. Trevisan, L. Prati, Pd on carbon nanotubes for liquid phase alcohol oxidation, *Catal. Today.* 150 (2010) 8–15.
- [43] K. Mori, T. Hara, T. Mizugaki, K. Ebitani, K. Kaneda, Hydroxyapatite-Supported Palladium Nanoclusters: A Highly Active Heterogeneous Catalyst for Selective Oxidation of Alcohols by Use of Molecular Oxygen, *J. Am. Chem. Soc.* 126 (2004) 10657–10666.
- [44] F. Sanchez, D. Motta, L. Bocelli, S. Albonetti, A. Roldan, C. Hammond, A. Villa, N. Dimitratos, Investigation of the Catalytic Performance of Pd/CNFs for Hydrogen Evolution from Additive-Free Formic Acid Decomposition, *C.* 4 (2018) 26.
- [45] S. Capelli, D. Motta, C. Evangelisti, N. Dimitratos, L. Prati, C. Pirola, A. Villa, Bio Adipic Acid Production from Sodium Muconate and Muconic Acid: A Comparison of two Systems, *ChemCatChem.* 11 (2019) 3075–3084.
- [46] M.L. Toebes, Y. Zhang, J. Hájek, T. Alexander Nijhuis, J.H. Bitter, A. Jos Van Dillen, D.Y. Murzin, D.C. Koningsberger, K.P. De Jong, Support effects in the hydrogenation of cinnamaldehyde over carbon nanofiber-supported platinum catalysts: Characterization and catalysis, *J. Catal.* 226 (2004) 215–225.